Experimentally-Validated Micromixing-Based CFD Model for Fed-Batch Stirred-Tank Reactors

Otute Akiti and Piero M. Armenante
Otto H. York Dept of Chemical Engineering, New Jersey Institute of Technology, Newark, NJ 07102

A model was developed to predict the final product distribution in fed-batch, stirred-tank reactors carrying out fast, parallel, chemical reactions, and the predictions were compared with experimental data. The following reaction system was chosen:

$$A + B \xrightarrow{k_1} P + R$$

$$A + C \xrightarrow{k_2} Q + S$$

Comparison between the experimentally determined flow field inside the reactor, obtained with a laser-doppler velocimeter (LDV), and the predictions from computational fluid dynamics (CFD) simulations was favorable. A model was developed to predict the yield, X_S, of forming S from A, using CFD to describe the velocity distribution inside the reactor, two micromixing models to represent the interaction between turbulence effects and chemical reactions, and a multiphase model (Volume of Fluid (VOF) model) to track the reacting zone in a Lagrangian fashion. Model predictions for X_S were compared with experimental data. The agreement between the experiments and the results of the simulations was good. © 2004 American Institute of Chemical Engineers *AIChE J,* 50: 566–577, 2004
Keywords: CFD, LDV, micromixing, competitive reactions, fed-batch reactor

Introduction

The objective of this work is to quantify the effect of mixing on the final product distribution in fed batch, stirred-tank reactors where a limited reagent is slowly fed to the reactor and multiple, fast, parallel homogeneous reactions take place in the liquid phase. Fed-batch stirred-tank reactors are commonly encountered in industrial practice, and, especially, the pharmaceutical industry. The use of this type of reactors enables the operators to control temperature, helps prevent "runaway" reactions, and minimizes unwanted side reactions.

It has been extensively demonstrated experimentally that the final product distribution in complex reactive systems is greatly affected by the fluid dynamics of the reactors (Baldyga and Bourne, 1990). Hence, variables, such as impeller type and position, feed location, agitation intensity, and feed time of the limiting reactant have been shown to significantly alter the final concentrations of the reaction products (Bourne and Yu, 1994). This is especially the case when the characteristic times for the reactions are of the same order of magnitude as the characteristic blending time to homogenize the contents of the reactor. When the kinetics of the reactions are slow with respect to the blend time, the added reactant has sufficient time to be homogenized before the reactions can proceed to any meaningful degree: mixing in this case is not critical. However, when the reactions are "fast" the

Correspondence concerning this article should be addressed to P. M. Armenante at piero.armenante@njit.edu.
Current address of O. Akiti: Bristol-Myers Squibb Company, Pharmaceutical Research Institute, New Brunswick, NJ 08903; e-mail: otute.akiti@bms.com.

reactants may react as they become dispersed in the bulk of the liquid. Local inhomogeneities caused by the local depletion of some of the reactants affect the local reaction rates and, thus, mixing effects become important.

Most mixing problems occur in the scale-up stage, because the prevailing hydrodynamics in large vessels is different from that in smaller ones, where processes are developed. Mixing times in small vessels are typically short, and often shorter than the characteristic reaction times. This implies that reactions are more likely to take place in a homogeneous environment at this scale. Mixing times in large vessels (such as industrial reactors) are typically much larger. Undesired byproducts caused by mixing-sensitive reactions are more likely to be formed in large vessels than in small vessels, even if the same reactions are considered. Overdesigning rarely leads to a better process.

Computational fluid dynamics (CFD) has been successfully applied to model fluid flow in a variety of systems, including stirred tanks (Ranade and Joshi, 1990, 1989b; Brucato et al., 1994, 1998; Kresta and Wood, 1991; Armenante and Chou, 1996; Armenante et al., 1994). CFD involves the numerical solution of the conservation equations for mass and momentum, in the geometry of interest. The application of CFD to the study of turbulent flow in batch stirred-tank reactors where parallel chemical reactions are taking place is not straightforward, and the literature on the subject is sparse. In fact, CFD codes are currently unable to predict the product distribution in reactive flows exhibiting "fast" and "complex" chemistry. This is the result of the fact that CFD provides information about the bulk fluid flow, or macromixing, based on user-defined boundary conditions. Chemical reactions are molecular level processes, taking place at a microscale level that CFD does not resolve.

Micromixing models (Baldyga and Bourne, 1989a,b; 1984a,b,c; Bakker and van den Akker, 1994b, 1996) have been developed for the purpose of modeling the effect of mixing on chemical reactions at the molecular level. Micromixing models do not contain any information about the bulk flow (macromixing). A satisfactory means of linking information about the fluid dynamics to the kinetics is necessary in order to predict the outcome of complex reactive mixing systems.

A significant portion of the work involving the computational modeling of mixing and chemical reactions in stirred tanks is based on a network of zones formulation (David et al., 1992; Bourne and Yu, 1994; Wang and Mann, 1992; Baldyga and Bourne, 1988). Because this method requires experimentally derived correlations to describe the fluid flow, it is inadequate to investigate scale-up issues in novel systems. Work on modeling fast complex reaction systems with CFD was also conducted (Bakker and van den Akker, 1994b, 1996). The results reported were most encouraging. The method used was, however, unable to adequately predict the final product yield in all parts of the flow domain. A model was also recently presented where the effects of mixing on chemical reactions were modeled with CFD, without the use of a micromixing model (Brucato et al., 2000). Although the experimental data and the model predictions were in close agreement with each other, the peculiarity of the reaction system, and the formation of a solid precipitate during the reaction, make a direct comparison between those results, and the results of other investigators, difficult.

Therefore, the objective of this work was to develop a novel means of simulating the effect of mixing on chemical reactions in batch stirred-tank reactors, with existing models for macromixing and micromixing as building blocks. A new approach to link these two components was introduced so as to provide a general purpose tool that can be used to predict the product distribution of fast complex reactions in fed-batch stirred-tank reactors. All the numerical tools developed in this work were validated with original experimental data. In particular, experimental and numerical results are presented for a reactor, provided with a single pitched-blade turbine (PBT), and operated at different agitation speeds using two different micromixing models.

Reaction System

The parallel competing reaction set examined in this work was as follows (Bourne and Yu, 1994)

$$\underset{(A)}{\mathrm{NaOH}} + \underset{(B)}{\mathrm{HCl}} \xrightarrow{k_1} \underset{(P)}{\mathrm{NaCl}} + \underset{(R)}{\mathrm{H_2O}}$$

$$\underset{(A)}{\mathrm{NaOH}} + \underset{(C)}{\mathrm{CH_2ClCO_2C_2H_5}} \xrightarrow{k_2} \underset{(Q)}{\mathrm{CH_2ClCO_2Na}} + \underset{(S)}{\mathrm{C_2H_5OH}}$$

The rate constants k_1 and k_2 are, respectively, 1.3×10^8 $m^3/(mol \cdot s)$ and 0.0257 $m^3/(mol \cdot s)$ at 23°C (Bourne and Yu, 1991). The final product distribution is sensitive to hydrodynamic effects (Baldyga and Bourne, 1989b; Bourne and Yu, 1991, 1994), making this reaction set suitable for studying the effect of mixing and turbulence on chemical reactions. Of interest is the yield of forming S from A. If mixing is perfect, no segregation exists, and the yield of S from A, X_S, is given by

$$X_S = \frac{k_2 C_C}{k_2 C_C + k_1 C_B} \tag{1}$$

In such a case, X_S is practically zero for the above system of reactions because $k_1 \gg k_2$. When the segregation is intense (that is, the reactions take place independent of each other), the yield of S is not a function of the kinetics, and is given by

$$X_S = \frac{C_S}{C_P + C_S} = \frac{C_C}{C_B + C_C} \tag{2}$$

In such a case, if equal quantities of A, B, and C are reacted (as in this work), $X_S = 0.5$. Intermediate degrees of mixing intensity yield results between these two extremes, requiring the use of a micromixing model to describe the system.

Experimental Work

Experimental apparatus and method

The apparatus used in this work is shown in Figure 1. The reactor consisted of a flat-bottomed, cylindrical glass mixing vessel having an internal diameter, T, of 0.292 m, and fitted with four metal baffles (width: $0.1 \cdot T$) equally spaced around its periphery. Agitation was provided by a 93 W variable-speed motor (Model No. 455479, G. K. Heller Corp., Floral Park, NY) with a maximum agitation speed of 2,000 rpm. The

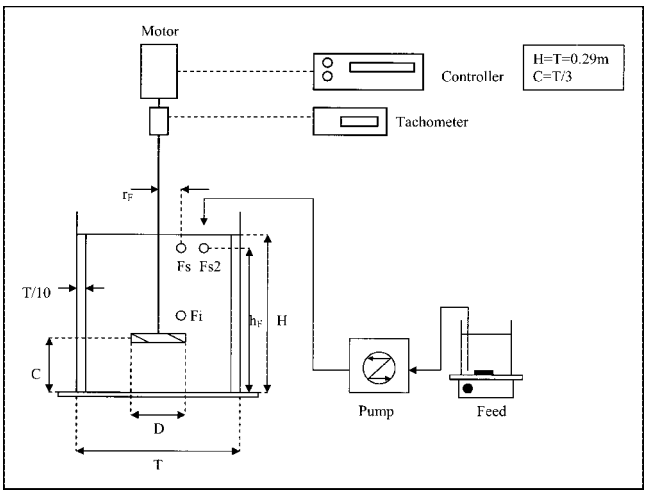

Figure 1. Experimental apparatus used in the reaction experiments.

rotational speed was measured with a digital tachometer, connected to a photoelectric pick-up sensor (Cole-Parmer, Chicago, IL), accurate to within ±1 rpm. The motor rotated a six-bladed pitched-blade turbine (PBT), with a 45° blade pitch, having a diameter D of 10.2 cm, and a vertically projected height of 1.2 cm. The clearance C of the impeller, off the tank bottom (measured from the middle of the impeller), was 1/3 of the vessel diameter.

The reactor was initially charged with aqueous solutions of two of the reagents, HCl and $CH_2CH_3CO_2Cl$ (Sigma-Aldrich, Milwaukee, WI), both with a resulting concentration of 18 mol/m^3, in the reactor. Before the introduction of the limiting reagent solution, (NaOH) the liquid level in the reactor H was equal to the vessel diameter. The NaOH solution (Sigma-Aldrich, Milwaukee, WI; feed concentration=900 mol/m^3; cumulative feed volume=1/50 of reactor volume) was then fed to the reactor, with a variable speed pump (Masterflex Model No. 7525–30, Cole Parmer, Chicago, IL) connected, via a flexible Tygon tube, to a glass tube with an outer diameter of 4.5 mm and an inner diameter of 3 mm. The initial temperature of all the solutions was always 23 ± 0.5 °C. No temperature control was in place. However, the temperature was recorded, but was never found to exceed 25 °C at the end of any experiment.

The total feed time was always 60 min, except in preliminary experiments aimed at determining the conditions under which micromixing was rate controlling (as discussed later in the section on Experimentally Determined Influence of Feed Time on X_S). Experiments were conducted at four different impeller speeds (100, 200, 300, and 400 rpm), using one of three different feed locations within the vessel, that is, just above the impeller (feed location "Fi": radial position, $r_{Fi}=0.172 \cdot T$; axial position, $h_{Fi}=0.48 \cdot H$), near the surface above the impeller ("F$_s$": $r_{Fs}=0.172 \cdot T$; $h_{Fs}=0.9 \cdot H$), or near the surface, midway between the shaft and the vessel wall ("Fs2": $r_{Fs2}=0.25 \cdot T$; $h_{Fs2}=0.9 \cdot H$) (Figure 1). The yield X_S was experimentally determined by measuring the concentration of ethanol, C_S, in the final product mixture. The concentration of ethylchloroacetate, C_C, was also measured to verify the mass balance. An HP 5890 Series II gas chromatograph, equipped with an FID detector (Hewlett Packard, Avondale, PA), and an Alltech packed column (1% AT–1,000 on 60/80 graphpac packing in a C–5,000 stainless steel casing, Alltech Associates, Deerfield, IL) was used for both analyses. The column temperature was programmed at 65 °C for 4 min, and then ramped at 10 °C/min to a final temperature of 150 °C, maintained for an additional 4 min. Calibration curves for both ethanol and ethylchloroacetate were obtained with standards of known concentrations.

The reaction experiments were always carried out in triplicate. The average error for X_S was found to be ±2.5%.

Experimental measurement of the flow field inside the reactor

The velocity flow field and turbulence intensity were experimentally determined with the Dantec 55X series Laser Doppler Velocimetry (LDV) apparatus shown in Figure 2 (Dantec Dynamics Inc. USA, Mahwah, NJ). The LDV systems consisted of a 750 mW argon-ion laser, producing a single multicolored laser beam that was passed through an optical filter to generate a monochromatic green beam (wavelength: 512 nm). A beam splitter produced two beams, one of which was passed through a Bragg cell to lower the frequency by 40 MHz and distinguish between positive and negative velocity measurements. The beams passed through a beam expander system and a focusing lens with a focal length of 330 mm, and intersected each other inside a clear Plexiglas cylindrical vessel, having the same geometric dimensions as the glass reactor used in the reaction experiments. The vessel was filled with water and then seeded with neutrally buoyant 1.5 μm silver coated particles (TSI, Inc., Minneapolis, MN) that could follow the fluid flow pattern very closely. The vessel was immersed in a clear Plexiglas square tank also filled with water to eliminate optical distortion. The vessel-tank assembly was mounted on an x-y-z traversing system that enabled the velocity to be measured everywhere within the vessel. The light scattered by the particles was collected by a photodetector assembly placed next to the tank at a 90° orientation with respect to the laser (Figure 2), and connected to a data acquisition system configured so as to take 5,000 measurements over a period of 60 s or less at the same location. The impeller agitation speed was 300 rpm. Data analysis was performed to generate the local mean and fluctu-

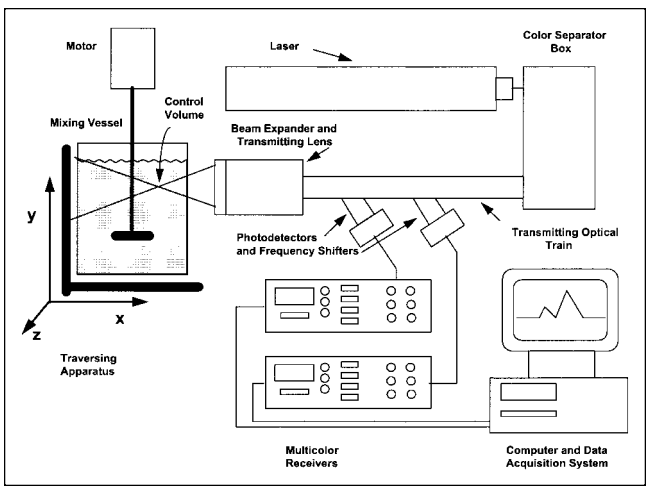

Figure 2. Laser Doppler Velocimetry System.

ating velocity components in the direction perpendicular to that of the plane of the two laser beams. Appropriate rotation of the laser beam assembly and translation of the vessel-tank assembly yielded the velocity components in all three directions at any location. The turbulent kinetic energy k was calculated from the experimental data as

$$k = \frac{1}{2}\left(u'^2 + v'^2 + w'^2\right) \tag{3}$$

All velocity measurements were made in triplicates. The average standard deviations of the axial, radial, and tangential velocities were found to be 11.7%, 13.7%, and 8.9%, respectively. The average standard deviation for the turbulent kinetic energy was 19.3%.

Model Formulation

As mentioned in the introduction, it has been shown before that it is possible to model the turbulent flow within an agitated vessel through CFD. It has also been previously shown that, with micromixing models, it is possible to simulate without approximation the influence of mixing on chemical reactions at the microscopic level (Baldyga and Bourne, 1984a,b). Missing from the picture is a means of linking the information provided by CFD at the macroscopic level, with that obtained from the micromixing models to produce a model that can be used to simulate and investigate the effects of mixing on chemical reactions. For such a model to be useful, it must be general enough such that no adjustable parameters are required and it must be numerically tractable, especially for three-dimensional (3-D) turbulent flows. It must also require a modest computational effort. There are presently no models in the open literature that satisfactorily meet these requirements. This contribution addresses the issue.

Modeling approach

The modeling approach was based on the use of a number of building blocks simulating different aspects of the mixing-reaction process, as follows: (1) the velocity distribution inside the reactor was first numerically determined; (2) the feed was numerically discretized into a finite number of elements, and each element considered individually as it was added to the reactor; (3) the expanding reaction zone resulting from the addition of a feed element was then numerically tracked as it moved and dispersed under the action of the flow field; (4) a micromixing model was introduced to account for the local level of turbulence; (5) a mass balance for each reactant was performed in the reaction zone (which, in principle, could even occupy the entire reactor), and the process was then repeated for the next feed elements until the feed was completely exhausted; and (6) the mass balance for the products over the entire addition time was carried out to finally determine their yields, and especially the yield of S from A, X_S. Each of these modeling building blocks is now examined in some detail.

Numerical simulation of the flow field via CFD

Numerical simulations of the velocity distribution inside the reactor (including its fluctuating components) were obtained with a commercially available CFD package (FLUENT v. 4.5.2). The full tank geometry (360°) was incorporated into the simulation. The computational domain consisted of 444,570 cells built from a 146 × 35 × 87 grid generated with the MIXSIM v.1.5 preprocessor (which is part of the FLUENT software). The impeller region of the grid was refined further from the MIXSIM default in order to better capture the steep gradients in velocity, and turbulence in that region. Similarly, the region of the grid near the tank bottom was also refined. Specifically, the number of axial grid lines used to describe the impeller region was increased from the MIXSIM default of three to 20. Ten additional grid lines were inserted near the tank bottom.

The *Reynolds Stress Model* (Rodi, 1984) was used to account for turbulence effects. Initially, a k-ϵ turbulence model was used. Although less computationally demanding, this model was found to underestimate significantly the turbulent kinetic energy obtained from LDV measurements. Therefore, it was abandoned. Other investigators who studied and compared the k-ϵ model to other turbulence models reached the same conclusions (Armenante and Chou, 1996; Armenante et al. 1997, Bakker and van den Akker, 1994a). There was no need to repeat those studies for this work. Pressure coupling was achieved with the *PISO* algorithm (Issa, 1985).

The impeller geometry was incorporated into the simulation by means of the Multiple Reference Frames (MRF) model (Luo et al., 1993; Luo et al., 1994). Although the MRF simulation is not time-dependent, it does overcome some of the problems associated with a completely steady state approach. The method works by dividing the volume into two domains, that is, an inner cylindrical domain including the impeller, and an outer domain, also comprising the baffles and the vessel wall, associated with the rest of the vessel. The inner domain is the source of the most unsteady flow because it contains the impeller, and it is modeled in a frame of reference rotating with the impeller. In this frame, the conservation equations are transformed into a rotating reference frame, and the flow is computed in a steady-state manner, thus treating an inherently time-dependent process as a steady-state flow. The outer domain is modeled as a steady-state process in a stationary reference frame. At the end of the computation, all the results are transformed back to the stationary reference frame.

The control volume technique employed in the solver involves the discretization of the computational domain into a finite number of contiguous control volumes. The equations of conservation are solved in sequence for each of these control volumes. Because the MRF formulation involves the solution of the model equations in two different frames of reference, it is possible that in some regions (in particular at the interface between the rotating reference frame and the stationary reference frame) the solution of a particular variable will depend on the values of other variables in portions of the solution domain that may not be in the same frame of reference. In such a situation, appropriate transformations from one frame to the other are performed to ensure that the solution is performed in a frame of reference, consistent with the variable of interest. The general velocity relationship for cells in two different frames of reference is given by

$$u_{i,N}^{\text{frame 1}} = u_{i,N}^{\text{frame 2}} + \varepsilon_{ijk}\left(\Omega_j^{\text{frame 2}} - \Omega_j^{\text{frame 1}}\right)x_k \tag{4}$$

where ϵ_{ijk} is the unit alternating tensor, Ω is the rotational speed of the reference frame (rad/s), and x_k is the Cartesian coordinate component. The second term on the righthand side of Eq. 4 is due to the different rotational speeds of the frames. The no-slip condition in the appropriate frame or reference was assumed at all solid surfaces.

The MRF approach enabled unsteady-state simulations to be carried out in a pseudo-steady-state manner. This translated into considerable savings in computer resources if compared to the more accurate, but time-consuming, fully time-dependent CFD simulation approach. In addition, the MRF approach allowed the possibility of including the complete impeller geometry into the computation without the necessity of using experimentally derived velocity profiles in the impeller region as boundary conditions for the impeller (Armenante et al., 1997).

The simulations were carried out on a Silicon Graphics International (SGI) Octane machine equipped with two MIPS R12000 64 bit processors, and 768 megabytes of random access memory (RAM). Each processor was equipped with 2 MB of cache memory. Additional computations were performed on an SGI Origin server equipped with 20 MIPS R120000 64 bit processors and 20 gigabytes of RAM.

A typical computational run to calculate the flow field in the entire vessel took 48–96 h, depending on the workload of the machines. The implementation of the VOF model took an additional 5–6 h to compute.

Feed discretization

The slow feed addition of a limiting reactant to a batch reactor is a continuous process. In order to mimic this process numerically, it is necessary to divide the feed into several feed elements that are fed, one at a time, sequentially into the vessel. This is what it is referred to here as feed discretization. Discretization was numerically accomplished by dividing the cumulative feed-volume into a number (σ) of identical feed elements, each having a volume equal to $1/\sigma^{\text{th}}$ the total feed volume. When a feed element was introduced in the reactor, it was allowed to react until consumed, as described below. Then, the process was repeated with successive elements until all the feed was consumed. Simulations were conducted in which only σ was varied, in order to determine the minimum value of σ for which the reactants were independent of σ. This approach works because the feed rate used in the experiments was *slow*, thus allowing for the numerical treatment of each feed element independent of all the others, that is, without interactions from other feed elements.

Tracking the reaction zone and calculation of ϵ_r and k_r via a pseudo-multiphase model (VOF model)

Visualization studies have shown that, for a system of the type described in this work, the reaction zone moves away from the feed location, whereas the reaction takes place as a result of bulk motion and micromixing (Bourne et al., 1995). Consequently, the moving reaction zone experiences varying levels of turbulent intensity, which, in turn, can affect the local concentration of the reactants because of micromixing effects, and, hence, the local reaction rates. Here, a multiphase model was used to represent the reacting fluid as a separate and distinct pseudophase having the same physical properties of the continuous phase. Defining the reaction zone as a separate phase merely serves to distinguish it from the bulk phase, and to keep track of its location as a function of time. The Volume of Fluid (VOF) model, a multiphase model designed for two or more fluids (Hirt and Nichols, 1981), was chosen because of its simplicity and modest computational requirements. The VOF model was implemented by solving a continuity equation for the volume fraction of the dispersed pseudophase in each cell of the computational domain

$$\frac{\partial \phi}{\partial t} + u_i \frac{\partial \phi}{\partial x_j} = S_\phi \tag{5}$$

where ϕ denotes the volume fraction of the reacting dispersed pseudophase. The source term S_ϕ can be constructed to simulate mass transfer between the phases. In this work, it was set equal to zero. In general, a single momentum equation is solved throughout the computational domain and the resulting velocity field is shared among the phases. The momentum equation is dependent on the volume fraction of each phase through the density and viscosity of each phase. Because these properties were identical for both the bulk and the reacting pseudophase, the momentum balance was not affected by the presence of the added reactant.

CFD was used to implement the VOF model. To simulate the dispersion effect of each added feed element, an appropriate number of cells (identified as the those cells surrounding the feed location, whose cumulative volume equaled the volume of the feed element) were initially numerically "filled" with the reacting pseudophase. Then, the dispersion process was followed in a Lagrangian fashion by determining the volume fraction of the dispersed pseudophase in each cell in the computational domain as a function of time. To do so, the time-averaged description of the turbulent flow field inside the reactor (previously determined through CFD in the absence of the dispersed phase) was used to compute the flows in and out of each cell, and, hence, the corresponding mass balance of the pseudophase in each cell. It was assumed that the introduction of feed material did not influence the flow field. Because the feed volume introduced into the system was a small fraction of the reactor volume, this is a reasonable assumption.

The VOF model was used not only to track the distribution of the reacting pseudophase as it moved within the vessel, but also to determine, at each time, the local value of the rate of dissipation of turbulent kinetic energy, ϵ, in each cell occupied, fully or partially by this phase, because ϵ is needed in the micromixing models, as described in the next section. The average value of ϵ for the entire reacting zone, denoted as $\bar{\epsilon}_r$, was calculated by taking the volume fraction average over all the cells occupied by the reacting fluid. Thus, at any time it was

$$\bar{\epsilon}_r = \frac{\int_{\substack{\text{Reactor}\\\text{Volume}}} \epsilon d(\phi V)}{\int_{\substack{\text{Reactor}\\\text{Volume}}} d(\phi V)} \cong \frac{\sum_{\text{All Cells}} \epsilon_i \cdot \phi_i V_i}{\sum_{\text{All Cells}} \phi_i V_i} \tag{6}$$

A similar approach was used to calculate the average turbulent kinetic energy in the reacting zone $\bar{k}_r$

$$\bar{k}_r = \frac{\int_{\substack{\text{Reactor}\\\text{Volume}}} k d(\phi V)}{\int_{\substack{\text{Reactor}\\\text{Volume}}} d(\phi V)} \cong \frac{\sum_{\text{All Cells}} k_i \cdot \phi_i V_i}{\sum_{\text{All Cells}} \phi_i V_i} \tag{7}$$

It was then possible to obtain $\bar{\epsilon}_r$ and $\bar{k}_r$ as a function of time for any given system.

Mass balances for the reactants using micromixing models

During this final computation step, that is, the calculation of the mass balances for all the reacting species and products, the reaction zone was treated as a segregated environment surrounded by perfectly mixed bulk fluid. The following mass balances were computed so as to determine the concentration of the generic species i undergoing engulfment in the entire reaction zone as a function of time

$$\frac{dC_i}{dt} = E(\langle C_i \rangle - C_i) + \sum_m r_m \tag{8}$$

where C_i and $\langle C_i \rangle$ are the concentrations of species i, respectively, in the reaction zone, and in the bulk fluid surrounding the reaction zone, and the index m denotes all the reactions in which species i is involved. For example, the mass balances for the three reacting species in this study are

$$\begin{aligned}
\frac{dC_A}{dt} &= E(\langle C_A \rangle - C_A) - k_1 C_A C_B - k_2 C_A C_C \\
\frac{dC_B}{dt} &= E(\langle C_B \rangle - C_B) - k_1 C_A C_B \\
\frac{dC_C}{dt} &= E(\langle C_C \rangle - C_C) - k_2 C_A C_C
\end{aligned} \tag{9}$$

The bulk concentrations $\langle C_i \rangle$ were kept constant throughout the integration of these differential equations for the entire time period τ, corresponding to the time the reactants added with a single feed element were nearly completely consumed (that is, when $C_i = 10^{-4}$ M). At the end of this time period, the overall mass balances for all the species in the entire reactor were conducted, and the new bulk concentrations were computed. The process was then repeated for another time period τ until the feed was completely used. In all cases it was found that $\tau \ll t_f/\sigma$, where t_f is the total feed time.

Micromixing models

Two different micromixing models were used to compute the engulfment parameter E required for the mass balance equations. The first micromixing model tested, the standard Engulfment Model (E-Model) developed by Baldyga and Bourne (Baldyga and Bourne, 1989a,b), computed E from the following equation

$$E = \frac{\ln 2}{\tau_\nu} = 0.058\left(\frac{\varepsilon}{\nu}\right)^{1/2} \tag{10}$$

where τ_ν is the lifetime of a vortex. The engulfment parameter depends on the state of turbulence through the local energy dissipation rate per unit liquid mass, ϵ. Here E was taken to be the average engulfment parameter for the *entire reaction zone,* and ϵ was substituted with $\bar{\epsilon}_r$. It should be stressed that $\bar{\epsilon}_r$ varies with time as the reaction zone moves and expands.

The second model used here was a Modified E-Model (Baldyga et al., 1997) in which mixing in the inertial convective range of the turbulent spectrum is also accounted for. Mixing in this range is more commonly referred to as mesomixing, an intermediate stage of mixing between macromixing and micromixing by engulfment. In the Modified E-Model the rate of growth of the micromixed volume is given by the following expression

$$\frac{dV_B}{dt} = EV_B\left[1 - \frac{V_B \exp(-t/\tau_s)}{V_s}\right] \tag{11}$$

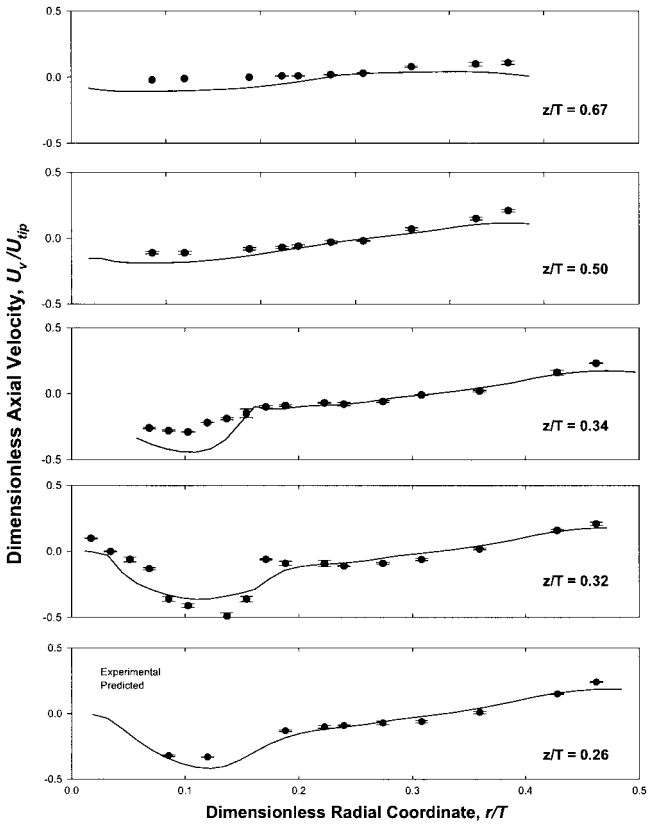

Figure 3. Comparison between experimental *axial* velocity measurements (via LDV), and numerical predictions (via CFD), at five horizontal positions ($z/T = z/H$), with the RSM turbulence model (N=300 rpm).

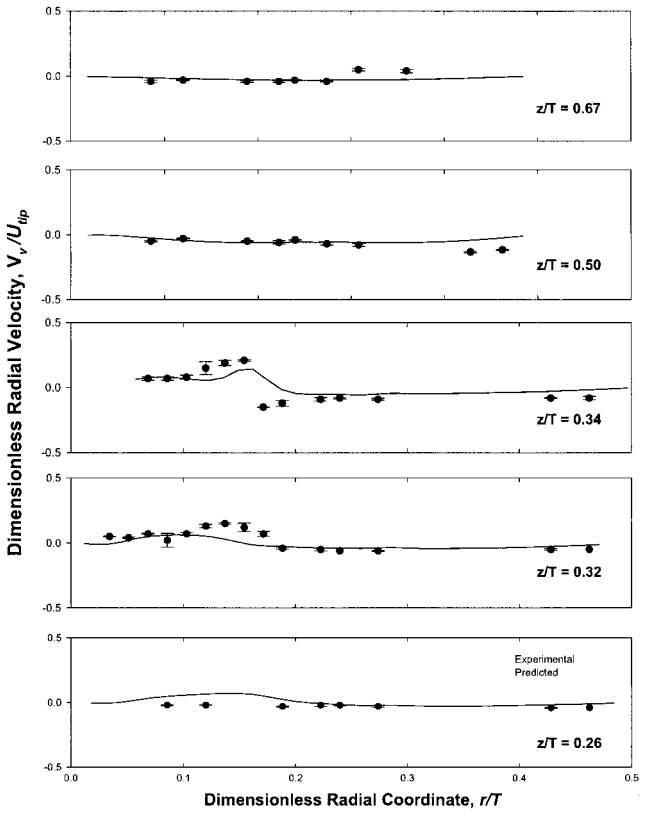

Figure 4. Comparison between experimental *radial* velocity measurements (via LDV), and numerical predictions (via CFD), at five horizontal positions ($z/T = z/H$) with the RSM turbulence model (N=300 rpm).

where V_B is the volume of fluid undergoing micromixing, $V_B=V_o$ when $t=0$, and V_o is the initial volume of the micromixed phase. The parameter τ_s represents the time constant for mesomixing and was taken here to be given by the expression (Baldyga et al., 1997)

$$\tau_s \equiv \frac{k}{\varepsilon} \tag{12}$$

The use of these equations yields the following expression for the engulfment parameter E'

$$E' = 0.058\left(\frac{\varepsilon}{\nu}\right)^{1/2}\left[1 - \frac{V_B \exp(-t/\tau_s)}{V_s}\right] \tag{13}$$

In this formulation E' depends not only on the local energy dissipation rate per unit liquid mass, ϵ, but also on the local turbulent kinetic energy k. As in the previous case, E' was taken to be the engulfment parameter for the entire reaction zone. Therefore, ϵ was substituted with $\bar{\epsilon}_r$, and k with $\bar{k}_r$ in Eq. 13.

Determination of X_s as a function of different operating variables

The final mass balance for product S was used to determine its final concentration at the end of the reaction process, and, hence, to calculate its yield X_s from reactant A. Numerical predictions were obtained for all the experiments conducted here with a pitched-blade turbine (that is, four agitation speeds, and three feed locations).

Results and Discussion

Comparison between experimental LDV velocity data and flow field CFD simulations

The results of the CFD simulation of the flow field were compared with the experimental LDV data for N=300 rpm. Figures 3, 4 and 5 show the results for the axial, radial, and tangential velocity components, respectively. The results for the turbulent kinetic energy are reported in Figure 6. Only data obtained at 300 rpm are shown here. In general, the predicted results, and experimental data appear to be in reasonable agreement. The simulation appears to capture all the most important features of the macroflow, especially the critically important features in the impeller region. For example, the down-pumping action of the impeller just above and below it is fairly well predicted, as shown in the axial velocity plot (Figure 3; z/T=0.32 and z/T=0.34). The predicted velocity profiles are in

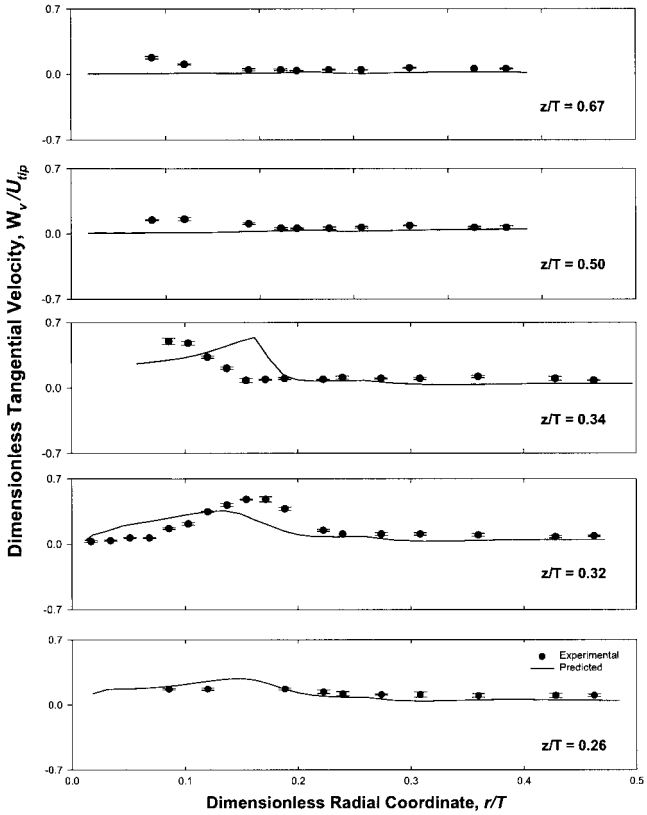

Figure 5. Comparison between experimental *tangential* velocity measurements (via LDV), and numerical predictions (via CFD) at five horizontal positions ($z/T = z/H$), with the RSM turbulence model (N=300 rpm).

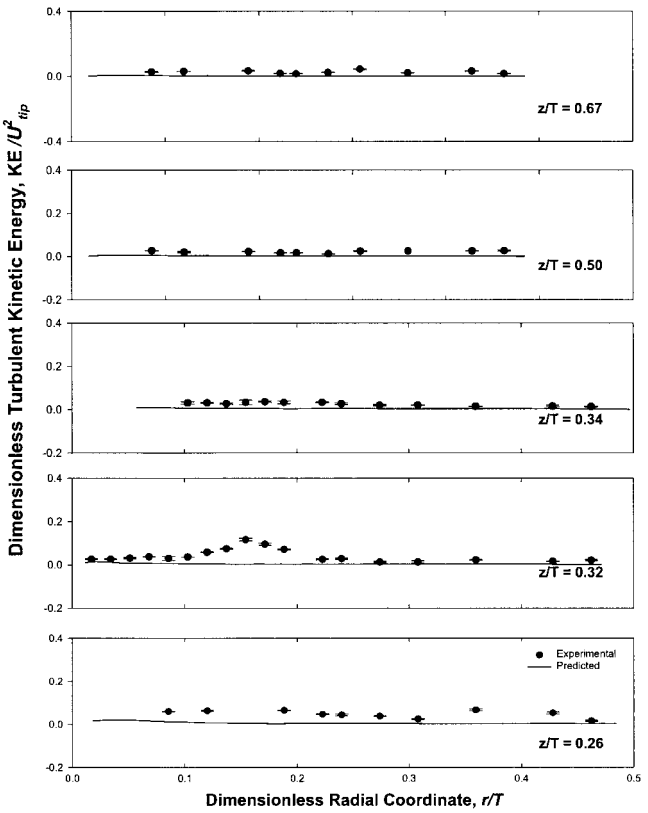

Figure 6. Comparison between experimental *turbulent kinetic energy* measurements (via LDV), and numerical predictions (via CFD) at five horizontal positions ($z/T = z/H$), with the RSM turbulence model (N=300 rpm).

good agreement with the results reported by Ranade and Joshi (1989) and Armenante and Chou (1996), who investigated similarly configured PBT-based systems. The strong downpumping action of the PBT, which is evidenced as the peak in the downward axial velocity at $r/T \approx 0.15$ above and below the impeller (Figure 3), was also reported in previous publications. Similarly, the drop in radial velocity just outside the impeller region (Figure 4; z/T=0.32 and z/T=0.34) is also qualitatively captured. The result for the tangential velocity near the impeller (Figure 5; z/T=0.32 and z/T=0.34) are less well predicted, although the results of the simulation are more similar to those that one would intuitively expect (such as an increasingly higher tangential velocity for $r<D/2$). Figure 7 shows a diagram of the predicted tridimensional flow field in the r-z plane.

Predicted distribution of the reacting pseudo-phase as a function of time

The distribution of the volume fraction ϕ of the reacting pseudophase was predicted in all simulations. Figures 8 and 9 show the typical evolution of the reaction zone with time for two different feed locations (Fs and Fi, respectively).

Results of chemical reaction experiments and model simulations

Experimentally Determined Influence of Feed Time on X_S. The feed time t_f used in the experimental work must exceed a

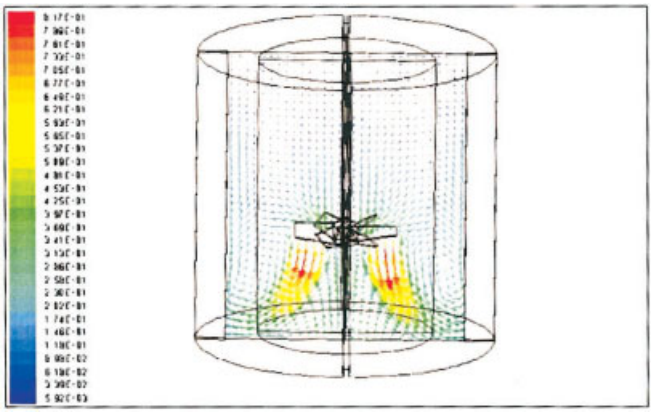

Figure 7. Tridimensional flow field in the *r-z* plane with FLUENT.

Velocity vectors are indicated by arrows. Maximum velocity = 0.8167 m/s (red) and minimum velocity = 0.0059 m/s (blue).

critical feed-time t_{crit} to ensure that the experiments are carried out in a micromixing-controlled regime (Baldyga and Bourne, 1989a,b). Ideally, t_{crit} should be determined for each set of experimental conditions. This is not realistic. A solution to this problem is to experimentally determine t_{crit} for the worst possible set of experimental conditions, that is, lowest agitation speed, highest initial concentration of reactant A, and a feed location near the surface (Bourne and Yu, 1991), where turbulence intensity is lower than at other feed locations. Then, this value of t_{crit} can be used for all the other less demanding experimental conditions. Figure 10 shows a plot of the experimentally determined X_S as a function of feed time (100 rpm; feed location near the surface Fs). For feed times longer than approximately 60 min, X_S was found to be independent of feedtime. Thus, t_{crit} was taken to be 60 min. This was the feed time used in all experiments.

Influence of Feed Discretization σ on Calculated X_S. In order to ensure that the results of the simulations were not affected by an incorrect choice of the value of the feed discretization parameter σ, preliminary simulations were conducted at different values of σ while keeping all other parameters in the simulations unaltered. The final value of X_S was calculated in all simulations. The results are reported in Figure 11 for the lowest (100 rpm), and highest (400 rpm) agitation speeds used in this work, and for two different feed locations (F*s* and Fi). This figure shows that when σ was larger than ~20, the results of the simulations did not change, even under

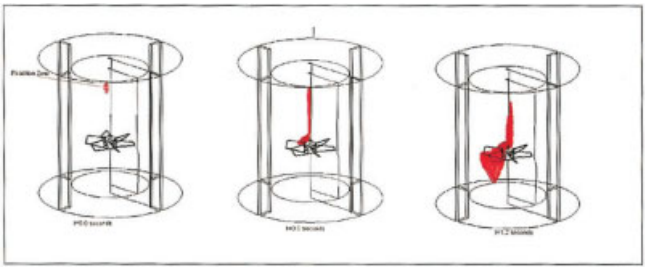

Figure 8. Trajectory of reaction zone for feed location Fs at 400 rpm.

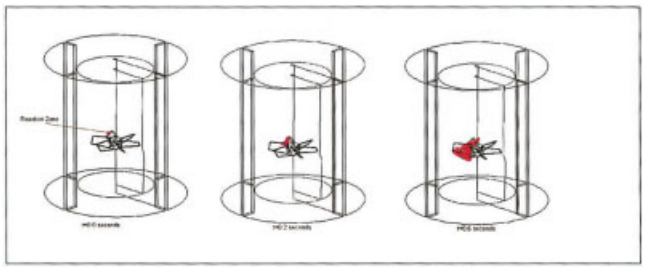

Figure 9. Trajectory of reaction zone for feed location Fi at 400 rpm.

the worst case scenario. Therefore, a value of 50 was used for σ in all the other simulations. This more than ensured that the computed yield was independent of discretization.

Reaction Time vs. Blend Time. The multiple reaction system under study is expected to be mixing-sensitive because the reaction time required to nearly complete the reactions is much shorter than the blend time to homogenize the feed into the bulk of the liquid. To verify that the model produced results that are consistent with this assumption, the depletion of the limiting reactant *A* (NaOH) in the reaction zone after the addition of a feed element was calculated as a function of time for different values of the agitation speed, feed location, and micromixing model used. The results are reported in Figure 12 (N=100 rpm) and Figure 13 (N=400 rpm). As anticipated, these figures show that the reactions proceeded more rapidly when the agitation speed was increased, and the feed was closer to the impeller. In addition, the Modified E-Model predicted a lower rate of consumption of the limiting reactant, because this model takes into account not only micromixing, but also mesomixing effects. From these figures, it was possible to calculate the reaction time to achieve nearly complete reactant consumption, defined here as the time required to consume 99.99% of the limiting reactant added with a single feed element. The reaction time was compared with the blend time to homogenize the liquid contents of the reactor, estimated from an experimentally derived correlation for pitched-blade turbines available from the literature (Ranade et al., 1991), in which the blend time was defined as the time to achieve 99% homogeneity. Even with the results obtained with the Modified E-Model, the reaction time for surface addition (Fs) at 100 rpm was found to be 2.9 s, compared to 27.2 s for the blend time. At 400 rpm, the reaction time and the blend time were calculated to be 1.05 s and 6.8 s, respectively. These results show that the primary reactant is predicted to be consumed in a time far shorter than the blend time to homogenize the system. Thus, the model successfully confirms that the reactants are depleted well before the vessel contents are homogenized, and that micromixing effects are expected to be important.

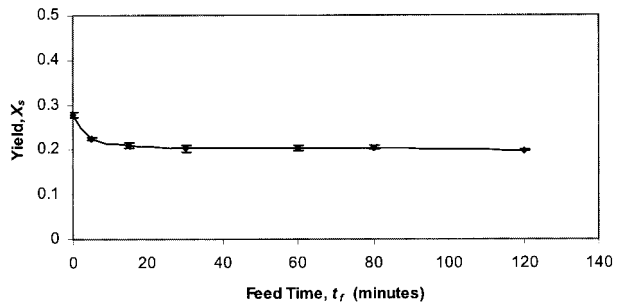

Figure 10. Variation of X_S with Feed Time for the PBT-based system (N=100 rpm; feed location near the surface, Fs).

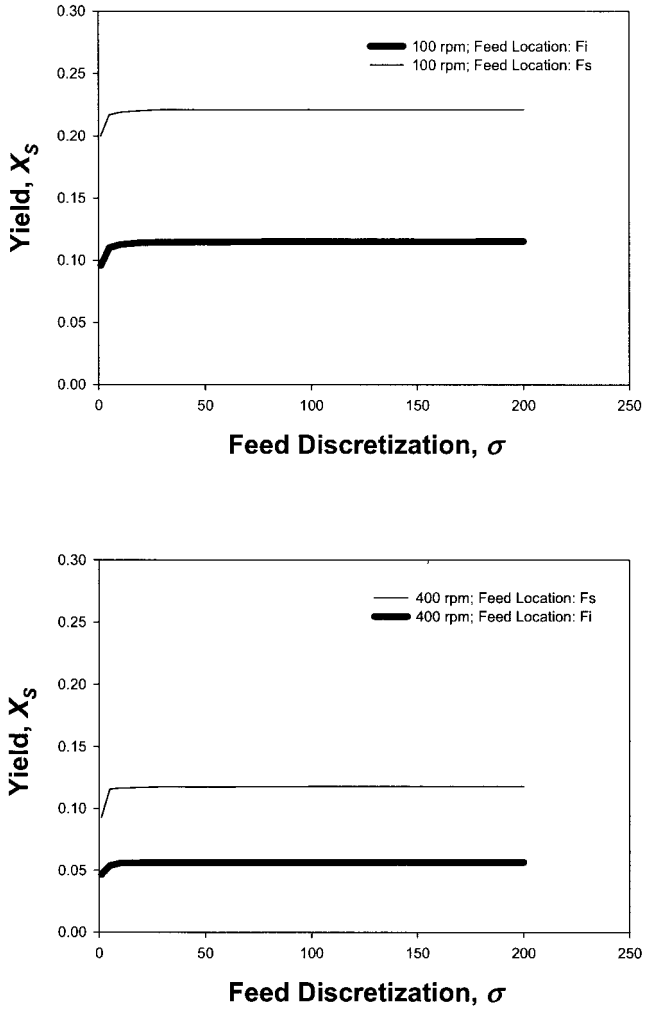

Figure 11. Effect of field discretization on the predicted yield X_s at different feed locations: N=100 rpm (upper panel); and N=400 rpm (lower panel).

Comparison between Experimental and Predicted X_S Values under Different Operating Conditions. The ultimate test of the validity of the proposed model is the comparison between the experimental and the calculated yield values. Figures 14, 15, and 16 show a comparison between the experimental data, and the model-predicted values of X_s as a function of the agitation speed N for three different feed locations, that is, *Fs*, Fs2, and Fi, respectively. In general, the agreement appears to be satisfactory, especially taking into consideration the complexity of the problem, the simplifying assumptions made, and the many components of the model. The agreement ranges from quite good, for the case of the surface feed location Fs, to acceptable, for the second feed location Fs2, to less satisfactory for the impeller feed location Fi. In all cases, the qualitative trend is captured.

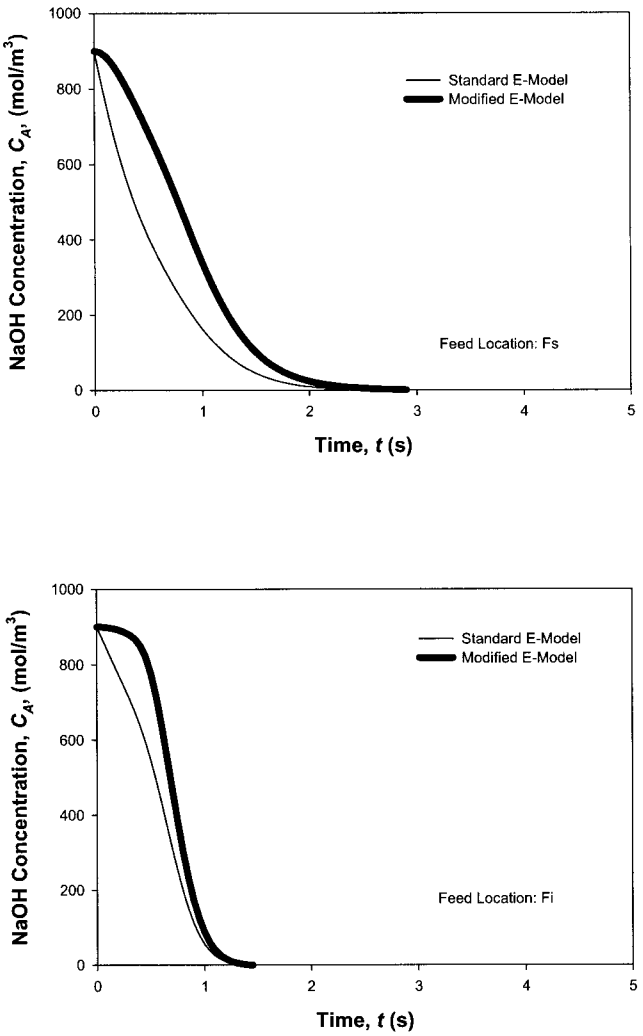

Figure 12. Predicted NaOH concentration in the reaction zone as a function of time following the addition of a feed element (N=100 rpm).

Feed location: Fs (upper panel); and Fi (lower panel).

Both the experimental data and the numerical predictions indicate that X_s decreases with increasing agitation speeds, as also reported in previous studies (Bourne and Yu, 1994; Bakker and van den Akker, 1994b, 1996). The predictions based on the use of the Modified E-Model were in general superior to those based on the standard E-Model. In some cases, as for the predictions for feed location Fs2, the improvement was quite significant.

When the feed was located in the highly turbulent region in the impeller suction stream (Fi), as opposed to near the liquid surface (Fs or Fs2), X_s was generally lower, at constant N. This is important for all those processes in which the kinetics of formation of the primary desired product is faster than that of a secondary undesired impurity, as in the reaction system examined here.

Conclusions

The numerical CFD predictions of the flow field in the reactor vessels were found to be in substantial agreement with experimental LDV data. The MRF modeling approach used here was not particularly demanding from a computational point of view, and did not require any experimentally-derived velocity boundary conditions for the impeller region.

With the MRF-based CFD model to simulate the flow field, it was possible to carry out simulations that accounted for all the major components of the reactor, including the impeller region, the vessel wall, and an accurate geometry of the impeller. This is not possible when impeller boundary conditions are used, because the impeller region is not properly modeled. Despite its modest computational requirements (as opposed to other time-dependent models), the MRF-based CFD model was able to capture all the major components of the flows, including those required by the overall model presented here to simulate the chemical reaction process. Therefore, its use currently appears to be an optimal compromise, at least for the time being, and for the application described in this study.

The results of this work indicate that a modeling approach based on the use of CFD simulation of the macroflow, coupled with a suitable micromixing model through the use of the VOF

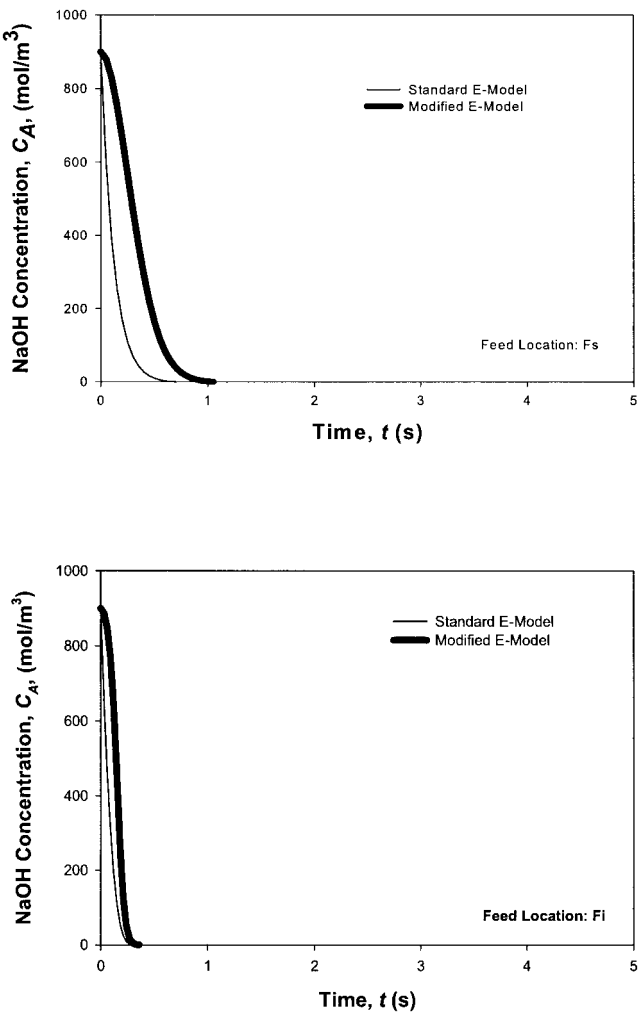

Figure 13. Predicted NaOH concentration in the reaction zone as a function of time following the addition of a feed element (N=400 rpm).

Feed location: Fs (upper panel); and Fi (lower panel).

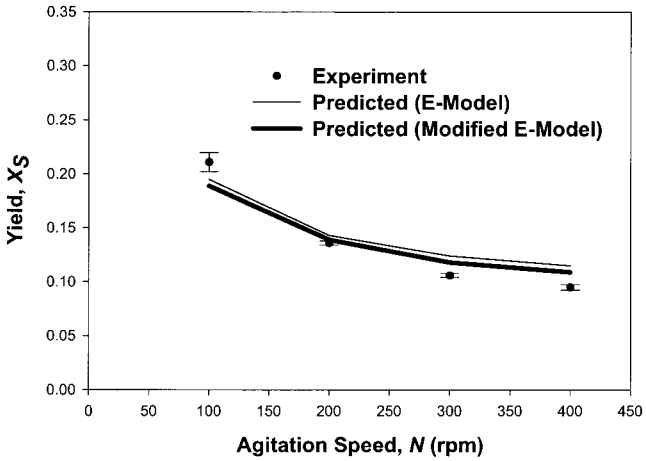

Figure 14. Effect of agitation speed on the predicted and experimental yield X_S.

Feed location: Fs.

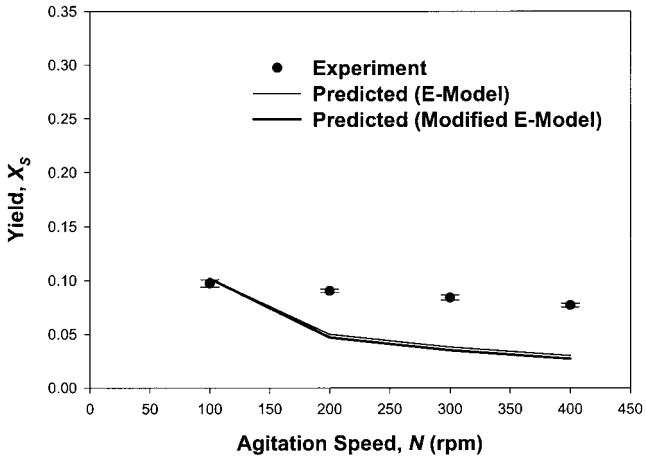

Figure 16. Effect of agitation speed on the predicted and experimental yield X_S.

Feed location: Fi.

model, can successfully predict the product distribution of reactions exhibiting complex chemistry in a fed-batch system. No experimental input was required for the implementation of the model and to predict the final product distribution. Experimental validation was obtained for a range of operating variables, including different agitation speeds and feed locations. The inclusion in the overall model of a modified micromixing model (partially incorporating mesomixing effects) resulted in a closer agreement with the experimental data, than when a standard micromixing model was used.

The agitation speed had the most significant impact on the yield X_S of the undesired species S: higher agitation speeds resulted in lower values of X_S, both experimentally and from model predictions. Varying the impeller location also resulted in significant experimental and predicted changes in X_S: feeding locations away from the impeller and closer to the liquid surface invariably resulted in lower yields. In conclusion, all the experimentally observed phenomena and trends were consistantly predicted by the model presented here. This work demonstrates that the effect of hydrodynamics on fast parallel reactions in stirred-tank reactors may be simulated with this novel computational tool. Because the approach proposed here does not require any adjustable parameters or experimental input, it is expected that its use could be extended to a wide variety of systems.

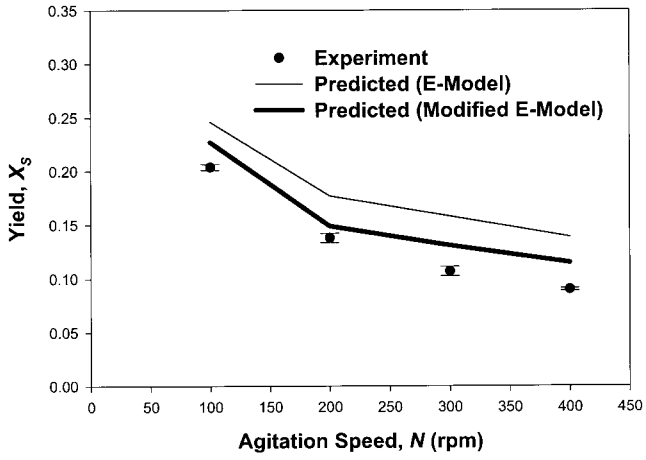

Figure 15. Effect of agitation speed on the predicted and experimental yield X_S.

Feed location: Fs2.

Acknowledgments

This work was partially supported by grants from the Bristol-Myers Squibb Pharmaceutical Research Institute (thanks to Dr. San Kiang), and Schering-Plough Corporation (thanks to Perry Lagonikos, Joseph Rogus, and Colin Walters). Their contribution is gratefully acknowledged. We would like to thank Schering-Plough Corporation (Joseph Rogus and Marc Steinman) for donating the LDV apparatus, and Fluent, Inc. (Dr. Elizabeth Marshall) for providing advice on CFD.

Notation

C = impeller clearance off vessel bottom, m
C_i = concentration of species i, moles/m^3
$\langle C_i \rangle$ = bulk concentration of species I, moles/m^3
D = impeller diameter, m
E = engulfment parameter, L/s
E' = modified engulfment parameter, L/s
H = height of liquid in vessel or reactor, m
k = turbulent kinetic energy, m^2/s^2
k_1 = kinetic constant of first reaction, m^3/(mol · s)
k_2 = kinetic constant of second reaction, m^3/(mol · s)
N = agitation speed, revolutions/min
R = vessel radius, m
t = time, s
t_f = feed time, s
T = vessel diameter, m
u_i = velocity vector, m/s
u_v = axial velocity, m/s
u' = axial fluctuating velocity, m/s
U_{tip} = impeller tip velocity, m/s
v_v = radial velocity, m/s
v' = radial fluctuating velocity, m/s
w_v = tangential velocity, m/s
w' = tangential fluctuating velocity, m/s
V = vessel volume, m^3
x_j = cartesian coordinate unit vector, m
X_S = yield of product S, dimensionless
z = axial location in vessel, m

Greek letters

ϕ = volumetric fraction of dispersed pseudophase, dimensionless
ϵ = turbulent energy dissipation rate, m^2/s^3
ν = kinematic viscosity, m^2/s
σ = number of discretized feed elements, dimensionless

Literature Cited

Akiti, O., and P. M. Armenante, "A Computational and Experimental Study of Mixing and Chemical Reaction in a Stirred Tank Reactor Equipped with a Down-pumping Hydrofoil Impeller Using a Micro-Mixing-Based CFD Model," *Proc.* 10th *Europ. Conf. on Mixing,* Delft, The Netherlands, Elsevier, New York, 61, (July 2–5, 2000).

Armenante, P. M, and C. C. Chou, "Velocity Profiles in a Baffled Vessel Provided with Single or Double Pitched-Blade Turbines," *AIChE J.*, **42,** 42 (1996).

Armenante, P. M., C.-C. Chou, and R. R. Hemrajani, "Comparison of Experimental and Numerical Fluid Velocity Distribution Profiles in an Unbaffled Mixing Vessel Provided with a Pitched-Blade Turbine," *I. Chem. Eng. Symp. Ser.,* No. 136, Cambridge, UK, 349 (1994).

Armenante, P. M., C. Luo, C.-C. Chou, I. Fort, and J. Medek, "Velocity Profiles in a Closed, Unbaffled Vessel: Comparison Between Experimental LDV Data and Numerical CFD Predictions," *Chem. Eng. Sci.*, **52**(20), 3483 (1997).

Bakker, A., and H. E. A. van den Akker, "Single-Phase Flow in Stirred Reactors," *Trans. I. Chem. Eng., Part A, Chem. Eng. Res. Des.,* **72,** 583 (1994a).

Bakker, R. A., and H. E. A. van den Akker, "A Computational Study of Chemical Reactors on the Basis of Micromixing Models," *Trans. I. Chem. Eng., Part A, Chem. Eng. Res. Des.,* **72,** 733 (1994b).

Bakker, R. A., and H. E. A. van den Akker, "A Lagrangian Description of Micromixing in a Stirred Tank Reactor Using 1D-Micromixing Models in a CFD Flow Field," *Chem. Eng. Sci.,* **51**(11), 2643 (1996).

Baldyga, J., and J. R. Bourne, "A Fluid Mechanical Approach to Turbulent Mixing and Chemical Reaction: Part I—Inadequacies of Available Methods," *Chem. Eng. Comm.,* **28,** 231 (1984a).

Baldyga, J., and J. R. Bourne, "A Fluid Mechanical Approach to Turbulent Mixing and Chemical Reaction: Part II—Micromixing in the Light of Turbulent Theory," *Chem. Eng. Comm.,* **28,** 243 (1984b).

Baldyga, J. and J. R. Bourne, "A Fluid Mechanical Approach to Turbulent Mixing and Chemical Reaction: Part III—Computational and Experimental Results for the New Micromixing Model," *Chem. Eng. Comm.,* **28,** 259 (1984c).

Baldyga, J., and J. R. Bourne, "Simplification of Micromixing Calculations I: Derivation and Application of New Model," *Chem. Eng. J.,* **42,** 83 (1989a).

Baldyga, J., and J. R. Bourne, "Simplification of Micromixing Calculations II: New Applications," *Chem. Eng. J.,* **42,** 93 (1989b).

Baldyga J., and J. R. Bourne, "The Effect of Micromixing on Parallel Reactions," *Chem. Eng. Sci.* **45,** 907 (1990).

Baldyga J., J. R. Bourne, and S. Hearn, "Interaction Between Chemical Reactions and Mixing on Various Scales," Chem. Eng. Sci., **52,** 457 (1997).

Bourne, J., R. Gholap, and V. Rewalkar, "The Influence of Viscosity on the Product Distribution of Fast Parallel Reactions," *Chem. Eng. J.*, **58,** 15 (1995).

Bourne, J. R., and S. Yu, "An Experimental Study of Micromixing Using Two Parallel Reactions," *Proc. 7th Europ. Conf. on Mixing,* Brugge, Belgium, **I**, 67 (1991).

Bourne, J. R., and S. Yu, "Investigation of Micromixing in Stirred Tank Reactors Using Parallel Reactions," *Ind. Eng. Chem. Res.*, **33**(1), 41 (1994).

Brucato, A., M. Ciofalo, F. Grisafi, and R. Tocco, "On the Simulation of Stirred Tank Reactors via Computational Fluid Dynamics," *Chem. Eng. Sci.*, **55**(2): 291 (2000).

Brucato, A., M. Ciofalo, F. Grisafi, and G. Micale, "Complete Numerical Simulation of Flow in Baffled Stirred Vessels: the Inner-Outer Approach," *I. Chem. Eng. Symp. Ser.,* No. 136, Cambridge, UK, 155 (1994).

Brucato, A., M. Ciofalo, F. Grisafi, and G. Micale, "Numerical Prediction of Flow Fields in Baffled Vessels: A Comparison of Alternative Modeling Approaches," *Chem. Eng. Sci.*, **53**(2) 3653 (1998).

Hirt, C. W., and B. D. Nichols, "Volume of Fluid (VOF) Method for the Dynamics of Free Boundaries," *J. Comput. Phys.*, **39:**201 (1981).

Issa, R. I., B. Ahmadi-Befrui, K. R. Beshay, and A. D. Gosman, "Solution of the Implicitly Discretized Reacting Flow Equations by Operator-Splitting," *J. Comput. Phys.* **93**(2), 388 (1991).

Kresta, S. M,. and P. E. Wood, "Prediction of the Three-Dimensional Turbulent Flow in Stirred Tanks," *AIChE J.*, **37**(3) 448 (1991).

Luo, J., A. Gosman, R. Issa, J. Middleton, and M. Fitzgerald, "Full Flow Field Computation of Mixing in Baffled Stirred Vessels," *Trans. I. Chem. Eng., Part A, Chem. Eng. Res. Des.,* **71,** 342 (1993).

Luo, J. Y., R. I. Issa, and A. D. Gosman, "Prediction of Impeller Induced Flows in Mixing Vessels Using Multiple Frames of Reference," *I. Chem. Eng. Symp. Ser.,* No. 136, Cambridge, U.K., 549 (1994).

Ranade, V. V., J. R. Bourne, and J. Joshi, "Fluid Mechanics and Blending in Agitated Tanks," *Chem. Eng. Sci.*, **46**(8), 1883 (1991).

Ranade, V. V., and J. B. Joshi, "Flow Generated by Pitched Blade Turbines I: Measurements Using Laser Doppler Anemometer," *Chem. Eng. Comm.,* **81**, 197 (1989a).

Ranade, V. V., and J. B. Joshi, "Flow Generated by Pitched Blade Turbines I: Simulation Using the k-ϵ Model," *Chem. Eng. Comm.,* **81**, 225 (1989b).

Ranade, V. V., and J. B. Joshi, "Flow Generated by a Disk Turbine: Part II. Mathematical Modeling and Comparison with Experimental Data," *Trans. I. Chem. Eng., Part A, Chem. Eng. Res. Des.,* **68,** 34 (1990).

Rodi, W., *Turbulent Models and Their Application in Hydraulics-A State of Art Review* 2nd ed., International Association for Hydraulic Research, Delft, The Netherlands, pp. 34–41 (1984).

Manuscript received Jan. 17, 2003, and revision received July 3, 2003